ORIGINAL RESEARCH ARTICLE

Dual-Band Bandpass Filter Based on Electromagnetic Coupling of Twin Square Metamaterial Resonators (SRRs) and Complementary Resonator (CSRR) for Wireless Communications

Mohammed Berka[1,2] · Hocine Abdelhak Azzeddine[1] · Amina Bendaoudi[2] · Zoubir Mahdjoub[2] · Ahmed Yacine Rouabhi[2]

Abstract

In this paper, a dual-band bandpass microwave filter (DBBPF) is presented. This filter is based on the electromagnetic coupling between two identical split-ring metamaterial resonators (SRRs) (for the same square shape and also for the same dimensions) and a complementary symmetrical metamaterial resonator (CSRR) for a square shape with optimized dimensions. The set of two square SRRs of magnetic activity for negative permeability ($\mu < 0$) and of the CSRR is etched on the upper face of a chosen substrate. The electrical qualities of our filter are improved by the electromagnetic inter-resonator coupling in the chosen optimum position and also by the coupling to the two microstrip feed lines. The results obtained based on simulations performed by the High-Frequency Structure Simulator (HFSS) commercial software show the impact of electromagnetic coupling between SRRs and the CSRR on our proposed filter. For the DBBPF without the CSRR, the two frequency bands are not so clear. But with the CSRR, the DBBPF filter becomes more selective, having two bandwidths 320 MHz and 280 MHz, respectively.

Keywords CSRR · dual-band bandpass · filter · metamaterial · refractive index · SRRs

Introduction

During the last decade, microwave circuits have experienced great development in terms of their electrical qualities. Among the devices most affected by this development, we note microwave filters and in particular bandpass and dual-band bandpass filters,[1–4] because these types of filters are frequently used in modern telecommunication systems.[5–7]

The electrical properties of microwave filters such as bandwidth, quality coefficient and selectivity represent the main focus of various studies.[8–10] In this context, several solutions have been proposed, including the filter approximation function,[11] the design technology[12] and also the choice of material for the microwave filter.[13–15] As a result,

a class of artificial materials has recently appeared, known as "Metamaterials".

The metamaterials studied by the Russian physicist Victor Veselago[16] are pseudo-homogeneous artificial or composite structures possessing electromagnetic properties not available in nature. These effective properties may have unusual values compared to homogeneous (conventional) materials. The particular property that has given this famous name "metamaterials" is the possibility of having simultaneously negative permittivity and permeability,[17] which leads to the most unexpected properties such as a negative refractive index.[18] Metamaterials derive their properties from the geometric structure of their inclusions, which allows them to be engineered in a wide frequency range that may go up to tens of THz.[19] This type of material has a very small structure (basic cell constituting the material) compared to the guided wavelength. It is accepted that the limit of homogeneity is set at sizes less than $\lambda_g/4$ which makes it possible to meet the need for the miniaturization of microwave circuits without a significant increase in electromagnetic loss.[20]

In this work, we present a miniaturized dual-band bandpass microwave filter based on two metamaterial split-ring

✉ Mohammed Berka
   mohammed_76_berka@yahoo.fr

1   Department of Electrotechnic, University of Mascara,
    Mascara, Algeria

2   EPO Laboratory, University of Sidi Bel Abbès,
    Sidi Bel Abbès, Algeria

resonators (SRRs) of a square shape for the same dimensions. Our approach is based on the impact of the electromagnetic coupling between these two SRRs and another proposed complementary symmetrical square metamaterial resonator (CSRR) (with optimized dimensions) which is etched on the same face of the used substrate. This CSRR is an element derived from the SRR. Geometrically, the CSRR also has very small dimensions compared to the wavelength. Physically, the CSRR for an arbitrary form is the complement of the SRR, i.e. all that are in conductive tracks in the SRR become slots in the CSRR and vice versa. Several studies have been carried out on this kind of element in various technologies (especially planar), but the most well known can be represented by Babinet's principle generalized by Booker.[21] Following this principle, the CSRR resonates when an electrical field is applied vertically to its plane. To have the effect of the CSRR, the global filter will be designed in two stages: the first filter design step will be without the slot (coupling of the two SRRs only) and the second will be with the slot (use of the CSRR). In a design with millimeter dimensions, the unusual electromagnetic characteristics of SRRs and the CSRR allows us to optimize the electrical qualities of our proposed microwave dual-band bandpass filter (DBBPF).

Design Approach

Depiction

The SRR is a metamaterial resonator proposed by Pendry and his research team.[22] Geometrically, the SRR is formed by two inner and outer split rings with two opposing interruptions to have a capacitive effect. Physically, the SRR can support small wavelengths of the order of a few micrometers.[23]

Square Split-Ring Resonator

The SRR square is a metamaterial resonator formed by two internal rings of radius R_1 and external rings of radius R_2 for a square shape. The period of the proposed (SRR) is P, l represents the spacing between the two rings which have the same width d, and the gaps are g. The square SRR works correctly when the magnetic field $\vec{H}$ is perpendicular to the plane of the two rings. Our square SRR and its equivalent electrical circuit are shown in Fig. 1.

The square SRR can be mainly considered as a magnetic dipole, its equivalent circuit model behaves like an L_0C_0 resonator excited by a magnetic field perpendicular to the plane of the rings.[24]
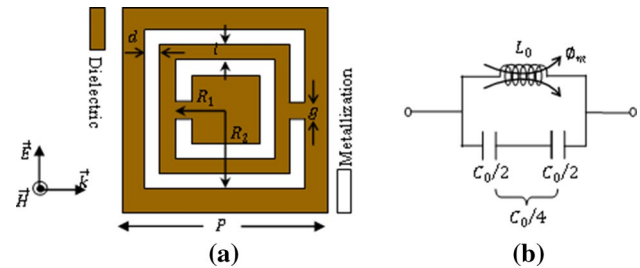

Fig. 1 Square SRR. (a) Representation in rings. (b) Equivalent electrical circuit.

Proposed Dimensions of the Square Split-Ring Resonator

To show the effect of geometrical parameters on the magnetic resonance of the square SRR, we are going to study three cells for different dimensions. The proposed dimensions for the square SRR are shown in Table I.

Proposed Dual-Band Bandpass Filter

Dual-Band Bandpass Filter Without the Slot

Our first proposed DBBPF consists of two square metamaterial SRRs. We choose the SRRs$_1$ to have the necessary miniaturization ($P_1 = 5.4$ mm). These two SRRs$_1$ are coupled in parallel with each other by an inter-resonator spacing which is e and a face length of one resonator from the other which is ($\theta_1 = R_2 = 2.35$ mm); they are fed by two microstrip lines of length ($l_m = 4.75$ mm) and width ($W = 0.96$ mm), and these input and output lines are coupled to the two SRRs$_1$ by spacing e_{in} and e_{out}, respectively, with ($e_{in} = e_{out} = 0.15$ mm). The overall size of our filter is obtained according to the external radius R_2 of each resonator SRR$_1$. We have carried out a parametric study according to three values of the spacing e ($e_1 = 0.15$ mm, $e_2 = 0.3$ mm and $e_3 = 0.45$ mm) and also according to the area (which depends on R_2) and the nature of the coupling (position of the gaps g). We treat two cases for our filter (DBBPF) without the slot; these two cases are represented by Fig. 2.

The surface of our filter (without slot) for both configurations is ($m \times n$) mm^2 with

$$\begin{cases} m = 2(S + W + +2R_2) + e_{in} + e_{out} + e \\ n = 2l_m + \theta_1 \end{cases} \quad (1)$$

We fix ($S = 3.2$ mm); the three surfaces of our filters (without slit) for the two configurations will be (18.17×11.85) mm^2 for e_1 spacing, (18.32×11.85) mm^2 for e_2 and (18.47×11.85) mm^2 for e_3.
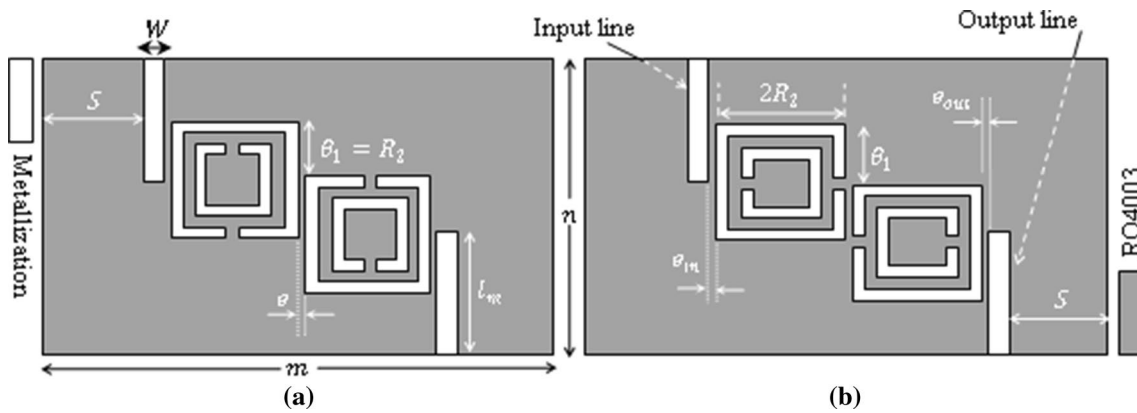
Fig. 2 Proposed DBBPF. (a) first configuration, (b) second configuration.

Dual-Band Bandpass Filter with CSRR

Our proposed DBBPF with the slot is constituted by two square $SRRs_1$ (the smallest resonators) and the slot represented by the proposed CSRR for a symmetrical square shape. For this filter, we choose the second configuration studied in the first case (filter without slot) in such a way that the two gaps of the two square $SRRs_1$ will be opposite each other to have the maximum of the electromagnetic coupling with ($\theta_1 = 0$ mm). The two $SRRs_1$ and the slot are spaced by the smallest value of the spacing ($e = e_1 = 0.15$ mm) to have an overall size which will be influenced by the use of a slot on the upper face of the substrate. The slot composed by the symmetrical square CSRR (which is placed in the optimal position) is located between the two $SRRs_1$, it has the length ($l_s = 2R_2 - 2g$) and the width ($W_s = Q - 2g$), where we have chosen ($Q = 7e_3 = 9g$). Our proposed DBBPF for this case is shown in Fig. 3.
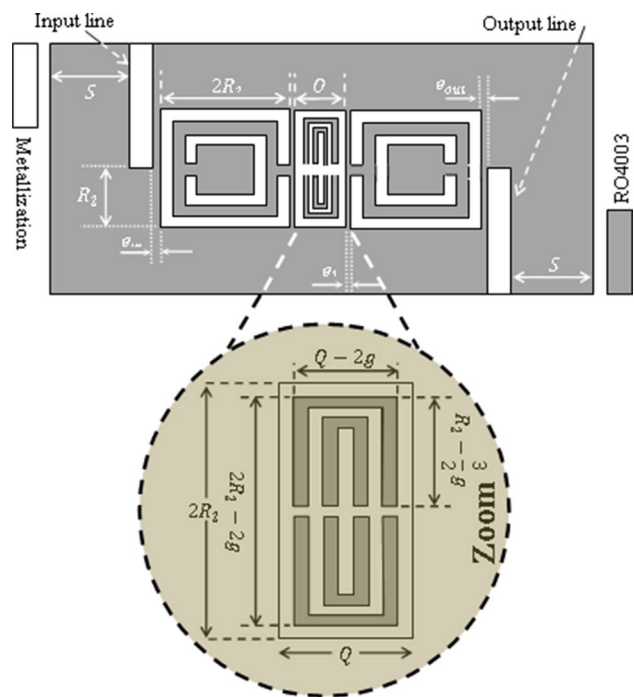
Results and Discussion

Square Split-Ring Resonator behavior

For a good use of the electromagnetic characteristics of the square SRR, we must choose the dielectric substrate on which we must etch our resonator. Since our SRR will be used for a filter structure, we must choose the type of substrate that is suitable for this kind of structure. In,[4] we have done a comparison between three types of dielectric substrate, while Rogers (RO4003) is the most suitable for our design. On the upper surface of this substrate ($\varepsilon_r = 3.55$; $tg\delta = 0.0027$), of thickness ($h = 0.85$ mm), the three square metamaterial resonators (SRRs) (for the chosen dimensions) are engraved for a thickness ($t = 15$ μm). One of the three squares (SRRs) (($SRR)_1$ in Table I) whose ($P_1 = 5.4$ mm) is

Fig. 3 DBBPF with the proposed CSRR.

shown in the 3-D Modeler of the High-Frequency Structure Simulator (HFSS), as shown in Fig. 4.

On the simulator, we polarize the three SRRs in the direction $\overrightarrow{OY}$ and we fix the boundary conditions on the fields (electric and magnetic, respectively). The boundary conditions for the simulation of our square SRR on the HFSS are maintained in our configuration (polarization along the $\overrightarrow{OY}$ axis) as follows. For the electric wall, we place PEC (Perfect Electrical Conductor) 1 and PEC 2 for the two faces perpendicular to the electric field $\vec{E}$, For the magnetic wall, we place PEM (Perfect Magnetic Conductor) 1 and PEM 2 for the two faces perpendicular

Parameter		g	l	d	R_1	R_2	P
Value (mm)	$(SRR)_1$	0.35	0.35	0.35	1.65	2.35	5.4
	$(SRR)_2$	0.65	0.65	0.65	1.95	3.25	7.8
	$(SRR)_3$	0.95	0.95	0.95	2.25	4.15	10.2

Table I Dimensions of the square SRR

to the magnetic field $\vec{H}$. For the two faces perpendicular to the direction of propagation, we place WAVEPORT1 and WAVEPORT 2, respectively.

The transmission coefficients of the three square SRRs are shown in Fig. 5.

Figure 5 shows the transmission coefficients of the three square SRRs over the [0-10] GHz frequency range. Note that the behavior of each studied metamaterial resonator is band-stop; the resonance of each square SRR is obtained according to its dimensions. So, for the smallest period we will have the most important magnetic resonance and vice versa (4.1 GHz for $P_3 = 10.2$ mm, 5.8 GHz for $P_2 = 7.8$ mm and 6.3 GHz for $P_1 = 5.4$ mm). The module and the phase of the SSR_1 are shown in Fig. 6.

The electromagnetic characteristics of SRR_1 are obtained by the variation of its permeability and its refractive index according to the frequency. The effective permeability of our metamaterial SRR_1 is given by the following expression.[25]

$$\mu_{\text{eff}}(f) = \frac{2}{jkh} \frac{1 - v_1}{1 + v_1} \tag{2}$$

where

$$v_1 = S_{21} - S_{11} \tag{3}$$

k is the wave number and it is equal to ω/c_0 (ω is the frequency in rad/s), and c_0 is the speed of light. h is the thickness of the substrate.

It follows that

$$\mu_{\text{eff}}(f) = \mu'_{\text{eff}} - j\mu''_{\text{eff}} = \frac{2}{jkh} \frac{1 - S_{21}(f) + S_{11}(f)}{(1 + S_{21}(f) - S_{11}(f))} \tag{4}$$

On the simulator, both the real and imaginary parts of the permeability are shown in Fig. 7.

Figure 7 shows the variation of the two real and imaginary parts of the effective permeability for the SRR_1 resonator. We note that the imaginary part of the permeability is positive along the frequency range of the simulation, while the real part changes its sign around the magnetic resonance of $SRR_{,1}$ which is 6.3 GHz. Then, the real part of the permeability is 8.31 at 6.25 GHz and −8.04 at 6.55 GHz. This behavior can define an important characteristic that contributes to improving the electrical qualities of the filter using our SRR_1 resonator, especially on the narrow band [6.25−6.55] GHz.

The refractive index of our resonator is defined by relation[25]

$$n_{\text{eff}}^2(f) = \mu_{\text{eff}}(f)\varepsilon_{\text{eff}}(f) \tag{5}$$

with

$$\varepsilon_{\text{eff}}(f) = \varepsilon'_{\text{eff}} - j\varepsilon''_{\text{eff}} = \frac{2}{jkh} \frac{1 - S_{21}(f) - S_{11}(f)}{(1 + S_{21}(f) + S_{11}(f))}. \tag{6}$$

The real and imaginary parts of the refractive index are shown in Fig. 8.

Figure 8 shows the variation of the two real and imaginary parts of the refractive index of the SRR_1 resonator. We note that, around the resonance of our SRR_1 and on the frequency range [5.85−6.95] GHz, the real part of the refractive index is negative, which gives us the physical characteristics of a left-hand metamaterial (LHM) medium. At the 6.3 GHz resonance, the refractive index is written $-6.63 + i\,0.65$, this characteristic, which does not exist for other types of resonators, can improve the electrical qualities of our proposed filter, especially for the minimization of losses.

The quality of the refractive index n of our SRR_1 is defined by its figure of merit (FOM), which can estimate the losses in this structure. The FOM is given by the following expression.[26]

$$FOM = -\frac{Re(n)}{Im(n)} \tag{7}$$

Figure 9 shows the FOM of the SRR_1.

In Fig. 9, we note that around the magnetic resonance of our SRR_1 (where the resonator is considered as a LHM), the FOM has high values of the order of 10.10 at the 6.3 GHz resonance, which indicates a low loss around this frequency. Also, these high values of the FOM provide better performance for our chosen metamaterial resonator (SRR_1), which allows the filter made up of these resonators to have optimized electrical qualities.

Frequency Response of the Proposed Dual-Band Bandpass Filter

Dual-Band Bandpass Filter Without Slot

Our proposed filter contains the two identical metamaterial resonators chosen after the previous study which are the

Table II Comparison of the performance of the designed filter with another work.

Works	Resonator structure	Center frequency (GHz)	IL(dB)	RL(dB)	Size (mm³)
[27]	Dual-behavior (DBR)	5/9	−0.44/−0.37	−17.0/−18.26	289.15
This work	SRRs and CSRR	5.02/8.92	−6.22/−5.23	−12.67/−20.78	173.31
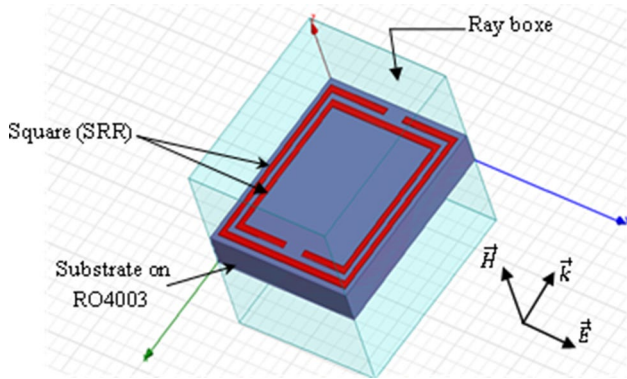
Fig. 4 Square SRR_1 polarization according to $\overrightarrow{OY}$.
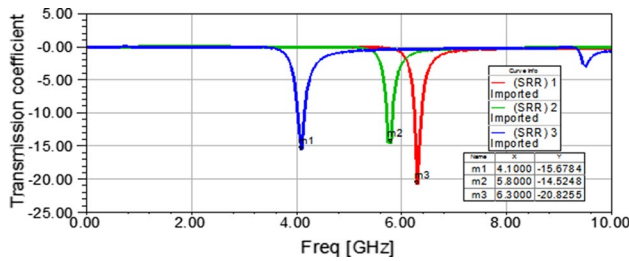
Fig. 5 Transmission coefficients for the three square SRRs.
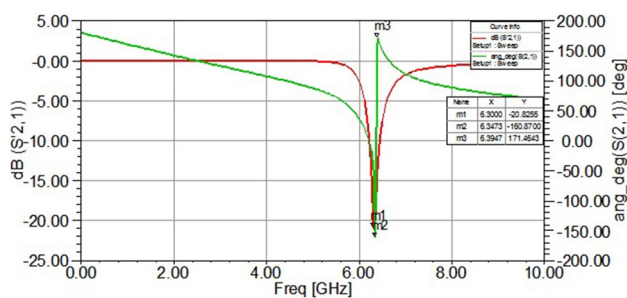
Fig. 6 SRR_1 transmission, module and phase.

Fig. 7 Permeability of square SRR_1 ; real and imaginary parts.
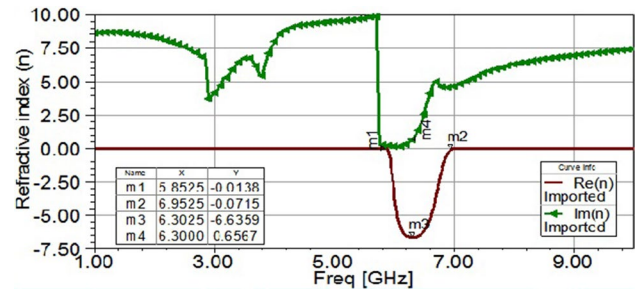
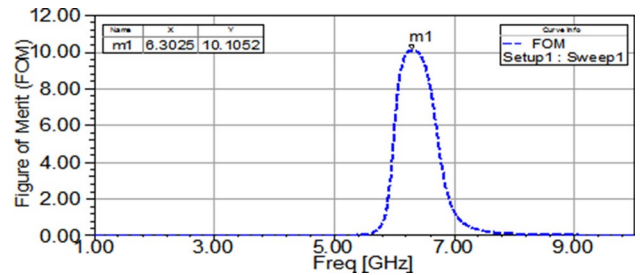**Fig. 8** Refractive index of square SRR_1, real and imaginary parts.

Fig. 9 Figure of merit (FOM).

The transmission coefficients of our DBBPF for the three inter-resonator spacings according to the two proposed configurations are shown in Figs. 11 and 12, respectively.

The transmission coefficients of the DBBPF without the slot shown in Figs. 11 and 12 show band-pass behavior with two bandwidths which are not so clear. A slight difference appears between the two behaviors for the two filter configurations. This difference is due to the position of the gaps in the two resonators (SRRs) constituting the filter.
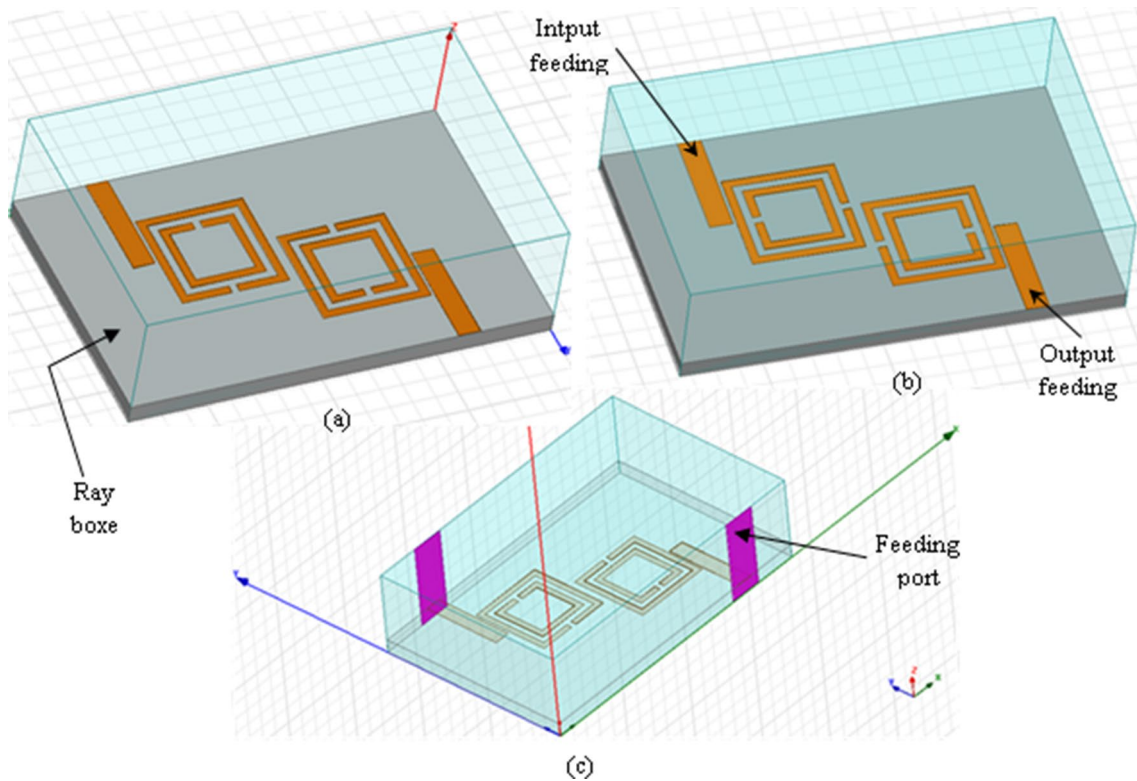
$SRRs_1$. For the two different configurations, our parametric study is based on the inter-resonator spacing (three simulations for e_1, e_2 and e_3). One of the three DBBPFs, which is without a slot (for spacing $e_3 = 0.45$ mm) is shown on the 3-D Modeler of HFSS in Fig. 10.

Fig. 10 DBBPF without CSRR for ($e_3 = 0.45$mm). (a) First configuration, (b) second configuration, (c) feeding ports.
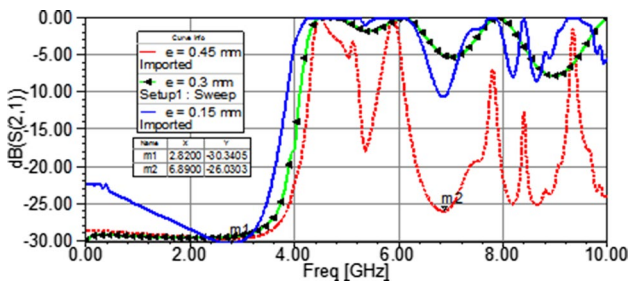

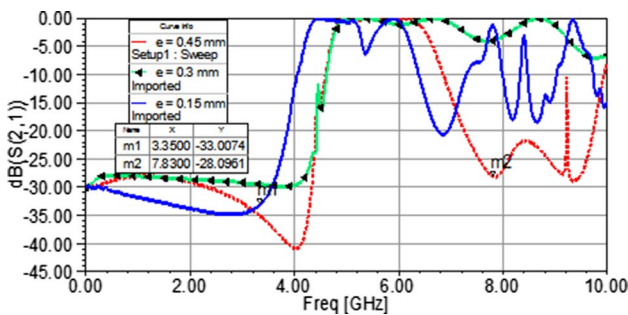**Fig. 11** Transmission of the DBBPF for the first configuration.

Fig. 12 Transmission of the DBBPF for the second configuration.

Dual-Band Bandpass Filter with the CSRR

The CSRR introduced between the two square SRRs (shown in Fig. 3) is placed in the optimal position to have the maximum electromagnetic coupling. The optimal position of the chosen CSRR is shown in Fig. 13.

We replace e by Q for the calculation of m and $\theta = 0$ for the calculation of n in (1), so the DBBPF with the proposed slot will have the following dimensions $m = 21.47$ mm and $n = 9.5$ mm (a surface of 203.9 mm^2 is less than the smallest size for the filter without the slot). The DBBPF with the proposed CSRR and its feeding ports are shown in Fig. 14.

The frequency response of our DBBPF is shown in Fig. 15.

Figure 15 represents the frequency response of our proposed DBBPF with CSRR. It is noted that it is a filter structure for two clear bandwidths; the first is of the order of 320MHz at the center frequency 5.02 GHz and the second of the order of 280 MHz at the center frequency 8.92 GHz. Between these two bandwidths, there is a rejection band of the order of 3.6 GHz. This rejection band is due to the use of our CSRR. We also note that, compared to the filter without the slot, our DBBPF with the CSRR becomes
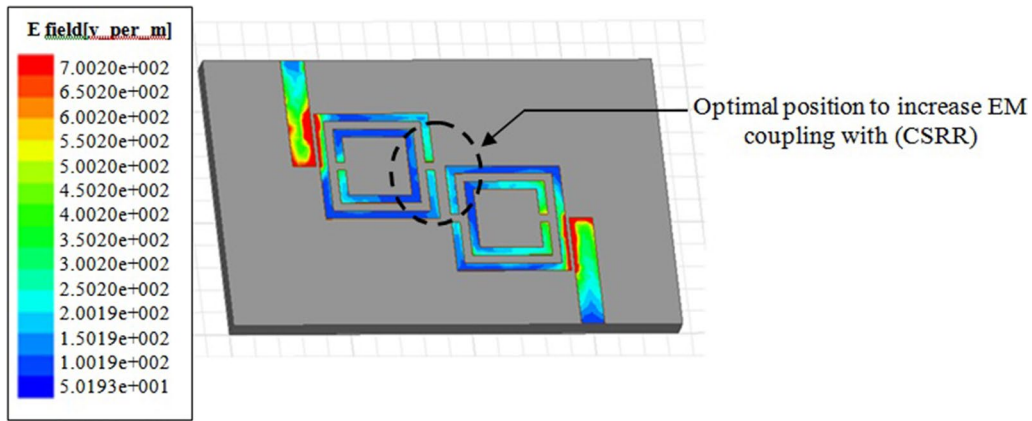
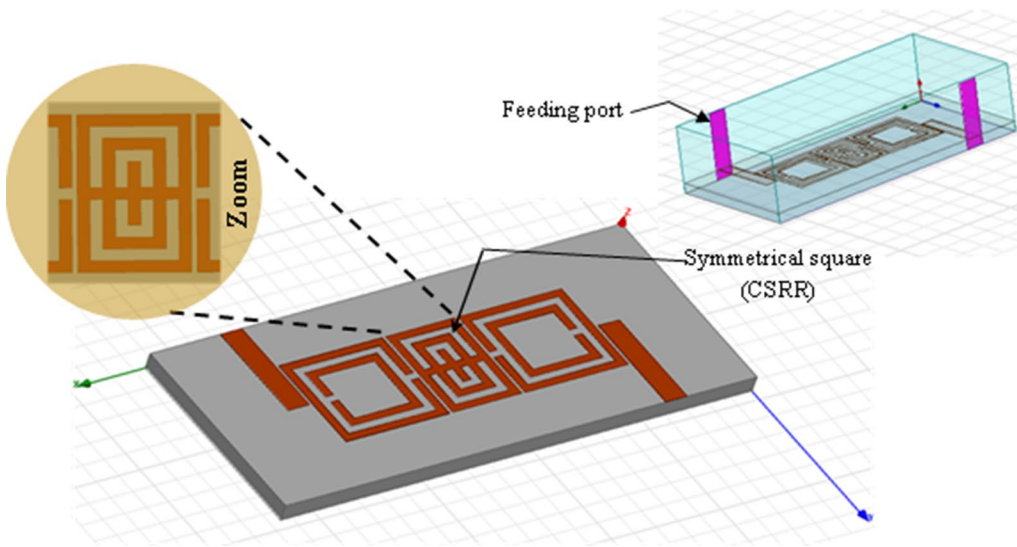**Fig. 13** Optimal position of the electromagnetic coupling with the CSRR.

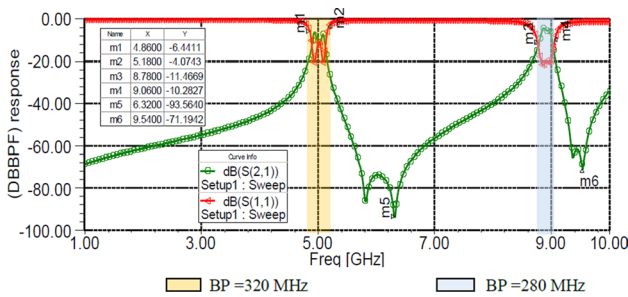**Fig. 14** 3-D view of the proposed DBBPF with CSRR.

Fig. 15 DBBPF response.

more selective for the two zero frequencies $f_{z1} = 6.32$ GHz and $f_{z1} = 9.54$ GHz.

The electric field distribution on our DBBPF at the two central frequencies is shown in Fig. 16.

The confinement of the electric field $\vec{E}$ at the two central frequencies for the two bandwidths is shown in Fig. 16. It is observed that the electric field is more confined in the region located between the SRRs and the CSRR, which justifies the desired electromagnetic coupling at the resonance frequencies for the two bandwidths. This coupling is responsible for the transfer of electromagnetic power from one metamaterial resonator to the other in the proposed filter.

We can compare the obtained results for the performance of our filter with another DBBPF in the same frequency regions. This comparison is summarized in Table II.
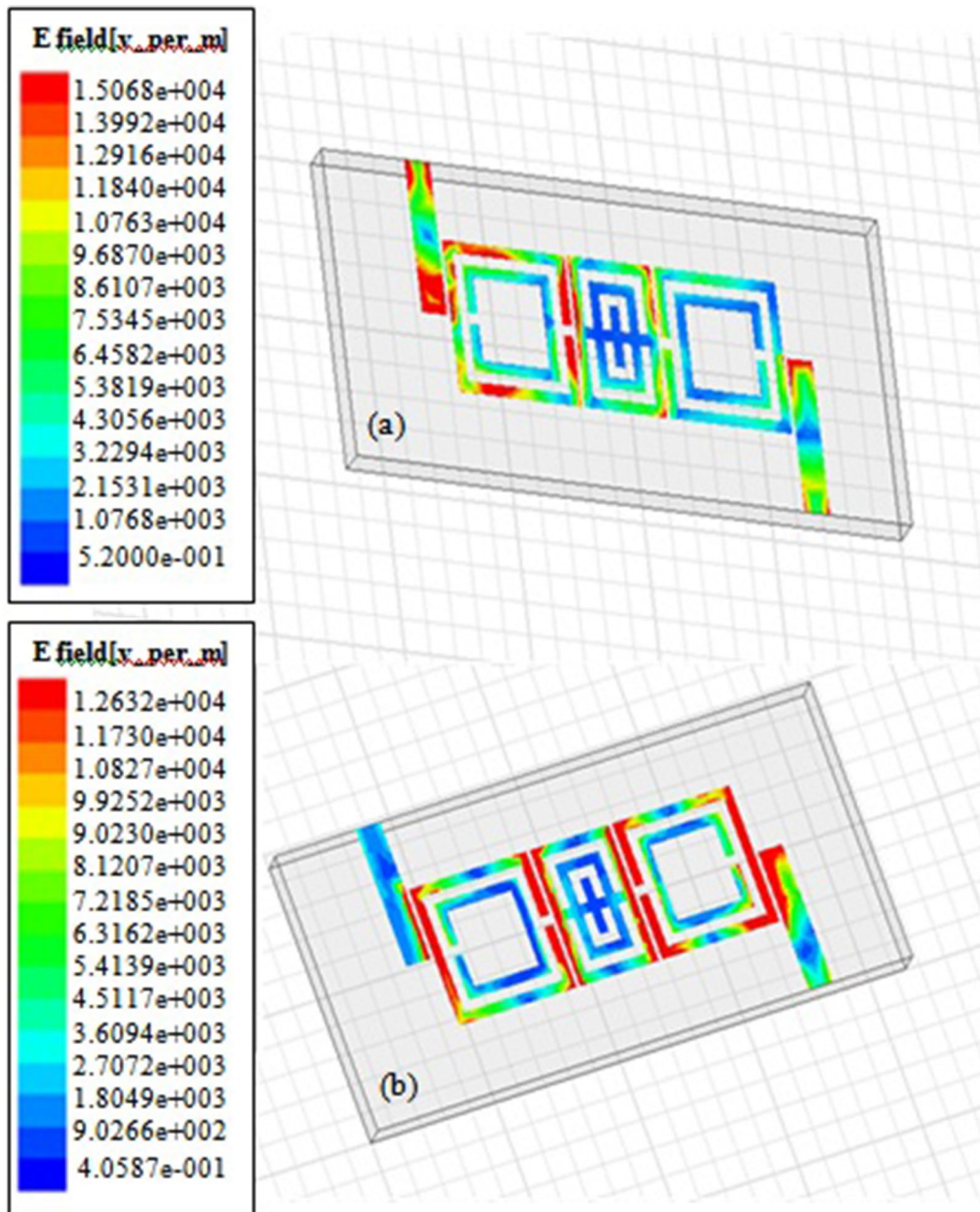
Fig. 16 Mapping of the electric field on the DBBPF at frequencies (a) $f_{01} = 5.02$ GHz, (b) $f_{02} = 8.92$ GHz.

Conclusions

In this work, a DBBPF based on ordinary SRRs and complementary CSRR metamaterial resonators is presented. By the beginning, we have presented the electromagnetic characteristics of the SRRs constituting our filter for a chosen square shape. For the DBBPF, we have passed through two steps; the first is dealing with proposing the filter with two SRRs only for two different configurations with a parallel coupling. These resonators have the smallest dimensions among the SRRs studied previously to have

the necessary miniaturization. In the second step, we have proposed introducing a symmetrical square slot based on a CSRR. The electric field distribution on the filter without the slot helped us to determine the optimal position to introduce our CSSR. When we have placed this CSRR between the two SRRs), our filter becomes more selective for two clear bandwidths on the order of 230 MHz and 280 MHz, respectively. These bandwidths are separated by a considerable rejection band which allows our DBBPF using the CSRR to operate without interference with other wireless communication systems.

References

1. P. Li, H. Chu, and R.S. Chen, *Elec. Lett.* 51, 1078 (2015).
2. Y.H. Song, G.-M. Yang, W. Geyi, and I.E.E.E. Microw, *Wireless. Comp. Lett.* 24, 230 (2014).
3. D. Huang and Z. Huang, *J. Elec. Comput. Eng.*, 2014, p. 1.
4. M. Berka, Z. Mahdjoub, and M. Hebali, *J. Elec. Eng.* 69, 311 (2018).
5. Y. Wu, X. Zhong, X. Xiong, and C. Liao, *J. Electromagnetic Waves Appl.* 27, 2176 (2013). https://doi.org/10.1080/09205071.2013.835702
6. Y. Wu, Q. Zeng, and Y. Shang, *Int. J. RF Microw. Comput. Aided.* 31, 22351 (2020).
7. E. Boria, B. Gimeno, S. Marini, M. Taroncher, S. Cogollos, P. Soto, A. Vidal, and J. Gil, *Int. J. RF. Microw Comput-Aid. Eng.* 17, 70 (2006).
8. K. Song, Y. Zhou, M. Fan, Y. Zhu, and Y. Fan, *Int. J. Microw. Wirel. Tech.* 9, 1931 (2017).
9. B. Belkadi, Z. Mahdjoub, M. Lamine Seddiki, and M. Nedil, *Turk. J. Elec. Eng. Comput. Sci.* 26, 2976 (2018).
10. A. Boutejdar, A. Omar, and P. Burte, *J. Microw. Opt. Electromagn. Appl.* 10, 295 (2011).
11. D. Milosavljevic, *AEÜ–Int J. Elect. Comm.* 59, 31 (2005).
12. A. Pourzadi, A. Isapour, and A. Kouki, *IEEE Trans. Microw. Theo. Tech.* 67, 1441 (2019).
13. C. Singh, Y. Bai, and B. Narang, *J. Elect. Materials.* 48, 6189 (2019).
14. X. Ya-wen, X. Jing-cheng, and L. Wei, *Infra. Phys. Tech.* 89, 398 (2018).
15. Z. Abolhasani, and M. Tayarani, *Iran. J. Elec. Electron. Eng.* 5, 230 (2009).
16. V.G. Veselago, *Sov. Phys. Uspekhi.* 10, 509 (1968).
17. D. Smith, W. Padilla, C. Vier, S. Nemat-Nasser, and S. Schultz, *Phys. Rev. Lett.* 84, 4184 (2000).
18. R.A. Shelby, D. Smith, and S. Schultz, *Sci.* 292, 77 (2001).
19. Y. Lin, K. Yan, D. Yao, and Y. Yu, *Opt. Las. Tech.* 11, 509 (2006).
20. H. Nguyen , J. Gauthier , J. M. Fernandez , M. Sierra Castañer and C. Caloz, *2006 Asia-Pacific Microw. Conf.*, 2006.
21. L. Thourel, *Ant. Cepadues.*, 1990, 2.
22. R. Marquez, F. Medina and R. Raffi, *Phys. Rev. B.*, 2002, 65.
23. R. Kumar Jaiswal, N. Pandit and N. Pathak, *2020 XXXIII Gen. Assem. Sci. Symp. Int. Uni. Rad. Sci.*, 2020.
24. R. Marqués, F. Mesa, J. Martel, and F. Medina, *IEEE Trans. Anten. Prop.* 51, 2572 (2003).
25. S. Hannan, M.T. Islam, A.F. Almutairi, and M. Faruque, *Sci. Rep.* 10, 1 (2020).
26. A.K. Panda, R.K. Mishra, and S. Sahu, *Microw. Opt. Technol. Lett.* 58 (2016). https://doi.org/10.1002/mop.29684
27. C. Hua, C. Miao, J. Xu, H. Wang, and W. Wu, *Microw. Opti. Tech. Lett.* 53, 731 (2011).